

Investigation of the ratio $\frac{\sigma_r}{F_2}(Q^2/s, Q^2)$ in the momentum-space approach

G.R. Boroun*

Department of Physics, Razi University, Kermanshah 67149, Iran

(Dated: February 12, 2026)

We present a calculation of the ratio $\frac{\sigma_r}{F_2}(x, Q^2)$ in momentum-space approach using the Block-Durand-Ha (BDH) parameterization of the proton structure function $F_2(x, Q^2)$. The results are compared with H1 data and extended to high inelasticity. We also examine the ratio $\frac{\sigma_r}{F_2}(\frac{Q^2}{s}, Q^2)$ obtained at a fixed \sqrt{s} and Q^2 to the minimum value of x given by Q^2/s , comparing them with both the HERA data and the color dipole model bounds. These results and comparisons with HERA data demonstrate that the suggested method for the ratio $\frac{\sigma_r}{F_2}$ can be applied in analyses of the Large Hadron Collider and Future Circular Collider projects. The effect of adding a simple higher twist term of the form F_2*H_2/Q^2 to the description of the ratio $\frac{\sigma_r}{F_2}(\frac{Q^2}{s}, Q^2)$ at low- x and low- Q^2 values for comparison with the color dipole bounds and the HERA data is investigated.

INTRODUCTION

The proton structure functions from the HERA collider summarize experimental efforts [1–3] conducted by the DESY collaborations H1 and ZEUS to significantly expand our understanding of the quark-gluon structure of the proton. These efforts reveal a sharp increase in $F_2(x, Q^2)$ at low values of x for a constant Q^2 , where pronounced scaling violations are observed. These violations are attributed to a high gluon density within the proton. Measurements of the inclusive deep-inelastic lepton-nucleon scattering (DIS) cross section have been essential for testing Quantum Chromodynamics (QCD) and provide us with an understanding of strong interaction dynamics.

The reduced cross section of the measured reaction $e^+p \rightarrow e^+X$ depends on the proton structure functions as:

$$\sigma_r(x, Q^2) \equiv F_2(x, Q^2) - \frac{y^2}{1 + (1 - y)^2} F_L(x, Q^2). \quad (1)$$

This dependence is on two independent kinematic variables, specifically chosen to be x and Q^2 , as well as on the center of mass energy squared s , with the inelasticity variable $y = Q^2/sx$. The new kinematic region with small values of the Bjorken variable x corresponds to the high energy (or Regge) limit of QCD extended to the Large Hadron electron Collider (LHeC) [4]. At LHeC, measurements are extended to much lower values of x and high Q^2 with $\sqrt{s} \simeq 1.3$ TeV, which is about 4 times the center-of-mass (COM) energy range of ep collisions at HERA. At low values of x , the DIS structure functions, which follow the relation $0 \leq F_L \leq F_2$ due to the positivity of the cross sections for longitudinally and transversely polarized photons scattering off protons, are defined solely by the singlet quark $xf_s(x, Q^2)$ and gluon density $xf_g(x, Q^2)$ as

$$F_k(x, Q^2) = \langle e^2 \rangle \sum_{a=s,g} \left[B_{k,a}(x) \otimes xf_a(x, Q^2) \right], \quad k = 2, L, \quad (2)$$

where $\langle e^2 \rangle = \sum_{i=1}^{n_f} e_i^2/n_f$ is the average charge squared for n_f which n_f denotes the number of effective massless flavours. The quantities $B_{k,a}(x)$ are the known Wilson coefficient functions and the parton densities satisfy the renormalization group evolution equations. The symbol \otimes indicates convolution over the variable x in the usual form, $f(x) \otimes g(x) = \int_x^1 \frac{dz}{z} f(z, \alpha_s) g(x/z)$.

The ratio σ_r/F_2 is defined by the following form at large values of the inelasticity

$$\frac{\sigma_r}{F_2}(x, Q^2) = 1 - \frac{y^2}{1 + (1 - y)^2} \frac{F_L}{F_2}(x, Q^2), \quad (3)$$

*Electronic address: boroun@razi.ac.ir

and in most of the kinematic range the relation

$$\frac{\sigma_r}{F_2}(x, Q^2) \approx 1, \quad (4)$$

holds to a very good approximation. Recently, the author in Ref.[5] has provided a definition the DIS structure functions at fixed \sqrt{s} and Q^2 to the minimum value of x given by Q^2/s with HERA data. We observe that the ratio σ_r/F_2 simplifies to the ratio F_L/F_2 at the kinematic point $x_{\min} = Q^2/s$ and $Q^2 \ll M_z^2$ by the following form

$$\frac{\sigma_r}{F_2}(Q^2/s, Q^2)|_{y=1} = 1 - \frac{F_L}{F_2}(Q^2/s, Q^2). \quad (5)$$

An interesting method for the DIS structure functions measurable in deeply inelastic scattering directly without unobservable parton distribution functions (PDFs) and without the associated scheme dependence in the momentum-space (MS) approach is presented in Ref.[6] and extended based on the Laplace transformation [7–11] in Refs.[12, 13]. The ratio of the F_L/F_2 is estimated to be less than 0.27 according to the color dipole model (CDM) bound in Ref.[14, 15], and the bound is lower than 0.27 with the ratio $\simeq 0.22$ in realistic dipole-proton cross section in Ref.[16]. The ratio of DIS structure functions is expressed in terms of the longitudinal-to-transverse ratio of the photo absorption cross sections in the CDM and defined in Ref.[17–20] by the following form

$$\frac{F_L(x, Q^2)}{F_2(x, Q^2)} = \frac{1}{1 + 2\rho(x, Q^2)}, \quad (6)$$

where factor 2 originates from the difference between the transverse and longitudinal photon wave function and the factor $\rho(x, Q^2)$ is related to the transverse-to-longitudinal ratio of the photoabsorbtion cross sections as

$$\rho(x, Q^2) = \frac{\sigma_T^{\gamma^* p}(W^2, Q^2)}{2\sigma_L^{\gamma^* p}(W^2, Q^2)}. \quad (7)$$

The transverse and longitudinal inelastic cross-sections in the dipole picture can be factorized in the following form

$$\sigma_{L,T}^{\gamma^* p}(x, Q^2) = \int dz d^2 \mathbf{r}_\perp |\Psi_\gamma^{L,T}(\mathbf{r}_\perp, z(1-z), Q^2)|^2 \sigma_{q\bar{q}}(\mathbf{r}_\perp, z(1-z), W^2), \quad (8)$$

where $\Psi_\gamma^{L,T}$ are the appropriate spin averaged light-cone wave functions of the photon and $\sigma_{q\bar{q}}(r, z, W^2)$ is the dipole cross-section which it related to the imaginary part of the $(q\bar{q})p$ forward scattering amplitude. The square of the photon wave function describes the probability for the occurrence of a $(q\bar{q})$ fluctuation [21–23]. The ratio of the DIS structure functions based on the value of ρ predicted to be 1 or $\frac{4}{3}$, as investigated in Refs.[24–29] can be used for the ratio σ_r/F_2 to be $\frac{2}{3}$ or $\frac{8}{11}$ respectively.

In this paper, we present the ratio σ_r/F_2 in a momentum-space approach using the proton structure function measurable in deeply inelastic scattering based on the Block-Durand-Ha (BDH) parameterization [7], which applies to large and small Q^2 and small x . The BDH parameterization provides a better fit to experimental data, particularly at low values of the Bjorken variable x . This improved fit is crucial for accurately describing the behavior of the proton structure function in regions where data is sparse. Additionally, the BDH parameterization aligns well with theoretical predictions, such as the Froissart bound, which describes the asymptotic behavior of hadron-hadron cross sections. By avoiding the need for a specific factorization scheme, the BDH parameterization simplifies the theoretical calculations involved in deep inelastic scattering processes, making them more efficient and accessible.

Firstly, we examine the ratio $\frac{\sigma_r}{F_2}(x, Q^2)$ due to the HERA center-of-mass (COM) energies, then we will extend the ratio to the limit $x_{\min} = Q^2/s$ which corresponds to high inelasticity $y = 1$, for comparison with the color dipole model bounds. By including an additional higher-twist term in the description of the ratio $\frac{\sigma_r}{F_2}(Q^2/s, Q^2)$, the results will improve at low- x and low- Q^2 values in comparison with the HERA data. The main goal of the paper is the ratio $\frac{\sigma_r}{F_2}(Q^2/s, Q^2)$ with the COM energies at the LHeC and EIC [30, 31] colliders. This ratio will define a limit bound for the data in these colliders.

METHOD

In this paper, the ratio σ_r/F_2 is determined directly in terms of observable quantities, specifically the proton structure function in DIS utilizing the BDH parameterization. The structure functions F_2 and F_L for deeply inelastic

scattering into the Parton Distribution Functions (PDFs) are defined in Ref.[6] by the following forms

$$\begin{aligned} F_2(x, Q^2) &= \langle e^2 \rangle \left\{ C_{2,s}^{(0)} + \frac{\alpha_s(\mu_r^2)}{2\pi} \left[C_{2,s}^{(1)} - \ln \left(\frac{\mu_r^2}{Q^2} \right) C_{2,s}^{(0)} \otimes P_{qq} \right] \right\} \otimes x \Sigma(x, \mu_r^2) \\ &\quad + 2 \sum_{i=1}^{n_f} e_i^2 \frac{\alpha_s(\mu_r^2)}{2\pi} \left[C_{2,g}^{(1)} - \ln \left(\frac{\mu_r^2}{Q^2} \right) C_{2,g}^{(0)} \otimes P_{qg} \right] \otimes x g(x, \mu_r^2), \end{aligned} \quad (9)$$

and

$$\begin{aligned} F_L(x, Q^2) &= \langle e^2 \rangle \left\{ C_{L,s}^{(1)} + \frac{\alpha_s(\mu_r^2)}{2\pi} \left[C_{L,s}^{(2)} - \ln \left(\frac{\mu_r^2}{Q^2} \right) C_{L,s}^{(1)} \otimes P_{qq} - 2n_f \ln \left(\frac{\mu_r^2}{Q^2} \right) C_{L,g}^{(1)} \otimes P_{gq} \right] \right\} \otimes x \Sigma(x, \mu_r^2) \\ &\quad + 2 \sum_{i=1}^{n_f} e_i^2 \frac{\alpha_s(\mu_r^2)}{2\pi} \left\{ C_{L,g}^{(1)} + \frac{\alpha_s(\mu_r^2)}{2\pi} \left[C_{L,g}^{(2)} - \ln \left(\frac{\mu_r^2}{Q^2} \right) C_{L,s}^{(1)} \otimes P_{qg} - \ln \left(\frac{\mu_r^2}{Q^2} \right) C_{L,g}^{(1)} \otimes P_{gg} \right] \right\} \otimes x g(x, \mu_r^2) \\ &\quad + \langle e^2 \rangle \left(\frac{\alpha_s(\mu_r^2)}{2\pi} \right)^2 \left[b_0 \ln \left(\frac{\mu_r^2}{Q^2} \right) \right] \left[C_{L,s}^{(1)} \otimes x \Sigma(x, \mu_r^2) + 2n_f C_{L,g}^{(1)} \otimes x g(x, \mu_r^2) \right], \end{aligned} \quad (10)$$

where C_{ij} ($i = 2, L$; $j = s, g$) denotes the scheme-dependent Wilson coefficient functions. The quark singlet and gluon PDFs can be expressed in terms of the DIS structure functions, therefore one of the explicit forms of the evolution equation is reported by the following form [6]:

$$\begin{aligned} \frac{dF_2(x, Q^2)}{d\ln Q^2} &= \frac{\alpha_s(Q^2)}{2\pi} x \left\{ \frac{1}{4} \left(\frac{2}{x} - \frac{d}{dx} \right) \frac{2\pi}{\alpha_s(Q^2)} F_L(x, Q^2) + \frac{1}{2} \int_x^1 dz \frac{2\pi}{z^2 \alpha_s(Q^2)} F_L(z, Q^2) \right. \\ &\quad \left. + C_F \left[\frac{1}{x} F_2(x, Q^2) - 2 \int_x^1 \frac{dz}{z^2} F_2(z, Q^2) + \frac{2}{x} \int_x^1 dz \frac{1}{(1-z)_+} F_2(\frac{x}{z}, Q^2) \right] \right\}, \end{aligned} \quad (11)$$

with the color factor $C_F = 4/3$ associated with the color group SU(3). The plus function is defined as

$$\int_x^1 dz \frac{f(z)}{(1-z)_+} = \int_x^1 dz \frac{f(z) - f(1)}{1-z} + f(1) \ln(1-x). \quad (12)$$

In Ref.[12], the authors developed a method to obtain the longitudinal structure function, F_L^{BH} , in the proton structure function and its derivative using a Laplace-transform method detailed in [7–11]. Then in Ref.[13], the authors modified the equation to significantly improve convergence for increasing numbers of terms in the series. Therefore, the ratio σ_r/F_2 is found to be

$$\begin{aligned} \frac{\sigma_r}{F_2}(x, Q^2) &= 1 - \frac{1}{F_2^{BDH}(x, Q^2)} \left\{ 4 \int_x^1 \frac{dF_2^{BDH}(z, Q^2)}{d\ln Q^2} \left(\frac{x}{z} \right)^{3/2} \left[\cos \left(\frac{\sqrt{7}}{2} \ln \frac{z}{x} \right) - \frac{\sqrt{7}}{7} \sin \left(\frac{\sqrt{7}}{2} \ln \frac{z}{x} \right) \right] \frac{dz}{z} - 4C_F \frac{\alpha_s(Q^2)}{2\pi} \right. \\ &\quad \times \int_x^1 F_2^{BDH}(z, Q^2) \left(\frac{x}{z} \right)^{3/2} \left[(1.6817 + 2\psi(1)) \cos \left(\frac{\sqrt{7}}{2} \ln \frac{z}{x} \right) + (2.9542 - 2\frac{\sqrt{7}}{7}\psi(1)) \sin \left(\frac{\sqrt{7}}{2} \ln \frac{z}{x} \right) \right] \frac{dz}{z} \\ &\quad + 8C_F \frac{\alpha_s(Q^2)}{2\pi} \left[\sum_{m=1}^{\infty} \left(\frac{2(m-4)}{m(m^2-3m+4)} - \frac{2}{m^2} \right) \int_x^1 F_2^{BDH}(z, Q^2) \left(\frac{x}{z} \right)^m \frac{dz}{z} \right. \\ &\quad \left. \left. + \int_x^1 F_2^{BDH}(z, Q^2) \left(\text{Li}_2 \left(\frac{x}{z} \right) - \ln(1 - \frac{x}{z}) \right) \frac{dz}{z} \right] \right\}, \end{aligned} \quad (13)$$

where the maximum value of m in the series is chosen to be approximately 50, with an accuracy of $1/10^4$, which is sufficient for the present purpose (please refer to the Appendix in Ref.[13]). The structure function $F_2^{BDH}(x, Q^2)$ has the following explicit expression:

$$F_2^{BDH}(x, Q^2) = D(Q^2)(1-x)^n \sum_{m=0}^2 A_m(Q^2) L^m, \quad (14)$$

with

$$\begin{aligned}
D(Q^2) &= \frac{Q^2(Q^2 + \lambda M^2)}{(Q^2 + M^2)^2}, \quad A_0 = a_{00} + a_{01}L_2, \quad A_i(Q^2) = \sum_{k=0}^2 a_{ik}L_2^k, \quad (i = 1, 2), \\
L &= \ln(1/x) + L_1, \quad L_1 = \ln \frac{Q^2}{Q^2 + \mu^2}, \quad L_2 = \ln \frac{Q^2 + \mu^2}{\mu^2},
\end{aligned} \tag{15}$$

where the effective parameters are summarized in Ref.[7] and are given in Table I.

In the limit where $x_{\min} = Q^2/s$ and it is indicated that the longitudinal polarization of the virtual photon at $y = 1$ is zero, we can conclude that the ratio $\frac{\sigma_r}{F_2}(Q^2/s, Q^2)|_{y=1} \rightarrow 1$. Therefore, we find that this ratio is defined by the following form:

$$\begin{aligned}
\frac{\sigma_r}{F_2}(Q^2/s, Q^2) &= 1 - \frac{1}{F_2^{BDH}(Q^2/s, Q^2)} \left\{ 4 \int_{Q^2/s}^1 \frac{dF_2^{BDH}(z, Q^2)}{d\ln Q^2} \left(\frac{Q^2}{sz} \right)^{3/2} \left[\cos \left(\frac{\sqrt{7}}{2} \ln \frac{sz}{Q^2} \right) - \frac{\sqrt{7}}{7} \sin \left(\frac{\sqrt{7}}{2} \ln \frac{sz}{Q^2} \right) \right] \frac{dz}{z} \right. \\
&\quad - 4C_F \frac{\alpha_s(Q^2)}{2\pi} \int_{Q^2/s}^1 F_2^{BDH}(z, Q^2) \left(\frac{Q^2}{sz} \right)^{3/2} \left[(1.6817 + 2\psi(1)) \cos \left(\frac{\sqrt{7}}{2} \ln \frac{sz}{Q^2} \right) \right. \\
&\quad \left. \left. + (2.9542 - 2\frac{\sqrt{7}}{7}\psi(1)) \sin \left(\frac{\sqrt{7}}{2} \ln \frac{sz}{Q^2} \right) \right] \frac{dz}{z} + 8C_F \frac{\alpha_s(Q^2)}{2\pi} \left[\sum_{m=1}^{\infty} \left(\frac{2(m-4)}{m(m^2-3m+4)} - \frac{2}{m^2} \right) \right. \\
&\quad \times \int_{Q^2/s}^1 F_2^{BDH}(z, Q^2) \left(\frac{Q^2}{sz} \right)^m \frac{dz}{z} + \int_{Q^2/s}^1 F_2^{BDH}(z, Q^2) \left(\text{Li}_2 \left(\frac{Q^2}{sz} \right) - \ln(1 - \frac{Q^2}{sz}) \right) \frac{dz}{z} \right\}.
\end{aligned} \tag{16}$$

In the following section, we calculated the ratio of $\frac{\sigma_r}{F_2}$ over a wide range of inelasticity based on the H1 data.

RESULTS AND CONCLUSION

With the explicit form of the ratio $\frac{\sigma_r}{F_2}$ (i.e., Eq. (13)), we begin to extract the numerical results at small x in a wide range of the inelasticity y , using the parametrization of $F_2^{BDH}(x, Q^2)$ (i.e., Eq. (14)). The QCD parameter Λ for four numbers of active flavor has been extracted [41] due to $\alpha_s(M_z^2) = 0.1166$ with respect to the LO form of $\alpha_s(Q^2)$ with $\Lambda = 136.8$ MeV. In order to account for the effect of the production threshold for the charm quark with $m_c = 1.29^{+0.077}_{-0.053}$ GeV [42, 43], the rescaling variable χ is defined by the form $\chi = x(1 + 4\frac{m_c^2}{Q^2})$ which is reduced to the Bjorken variable x at high Q^2 .

In Fig.1, we show the ratio of $\frac{\sigma_r}{F_2}$ based on the F_2 and F_L parametrizations in [7] and [12, 13], respectively. The comparison of the ratio with the H1 data [1] at moderate and low inelasticity is excellent according to the uncertainties. The ratio at large x (low inelasticity) is approaching unity. The ratio decreases from unity as inelasticity increases (very low x). This behavior is more pronounced at low Q^2 values. In Fig.1, we depict this behavior up to $y = 1$ as experimental data have not been determined in this region. The H1 data are selected in the region $1.5 \leq Q^2 \leq 45$ GeV 2 at the interval $0.518 \leq y \leq 0.004$. The importance of the longitudinal structure functions is evident in experimental data at low Q^2 values and high inelasticity, where the photon interaction becomes hadron-like in the CDM, as discussed in Ref. [25]. The error bars for the ratio $\frac{\sigma_r}{F_2}$ are determined by the following formula:

$$\Delta \left(\frac{\sigma_r}{F_2} \right) = \frac{\sigma_r}{F_2} \sqrt{\left(\frac{\Delta \sigma_r}{F_L} \right)^2 + \left(\frac{\Delta F_2}{F_2} \right)^2}, \tag{17}$$

where in the H1 data, $\Delta \sigma_r$ and ΔF_2 are obtained from the H1 experimental data [1]. In our calculations, the error bands depend on the uncertainties of $F_2(x, Q^2)$ and $F_L(x, Q^2)$ according to the parametrization coefficients in the BDH model (Table I) as follows:

$$\Delta \left(\frac{\sigma_r}{F_2} \right) = \frac{y^2}{Y_+} \frac{F_L}{F_2} \sqrt{\left(\frac{\Delta F_L}{F_L} \right)^2 + \left(\frac{\Delta F_2}{F_2} \right)^2}. \tag{18}$$

In Fig. 2, we present the prediction of Eq. (16) for the ratio $\frac{\sigma_r}{F_2}(\frac{Q^2}{s}, Q^2)$ and compare it with the results reported in

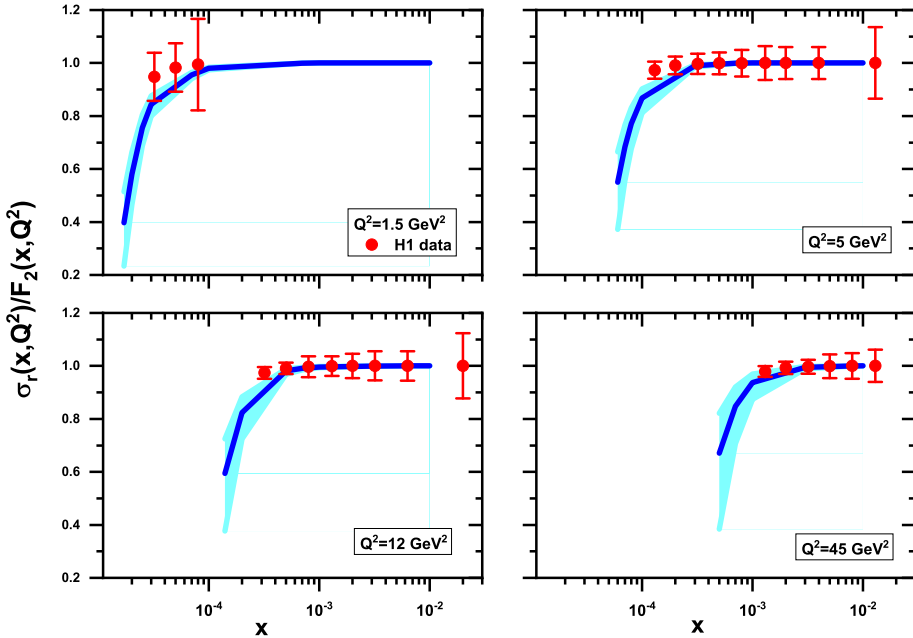


FIG. 1: The extracted ratio $\frac{\sigma_r}{F_2}$ (blue curves) from the parametrization methods is compared with the H1 data (red circles) [1]. The total errors, which account for both the reduced cross sections and the structure functions, are included. The error bands (cyan curves) of the ratio $\frac{\sigma_r}{F_2}$ correspond to the uncertainty in the parameterization of F_2 and F_L as shown in Table I.

Ref.[5] at $\sqrt{s} = 318$ GeV for $y = 1$, along with the data uncertainties. As shown in this figure, the values of the ratio are comparable to the data from Ref.[5] and are in good agreement with the CDM bounds over a wide range of Q^2 values. We also compared the ratio with the results proposed by the authors in Ref.[44] within the CDM in light of HERA high-precision data based on the impact parameter saturation model (IP-Sat) [45] and the BGK model [46]. According to the predictions of the DIS structure functions of models BGK and IP-Sat, there are only two data points with high inelasticity at $\sqrt{s} = 318$ GeV in Table IV of Ref.[44]. These results demonstrate good agreement between models and the MS approach.

Indeed, Fig.2 compares the HERA data in the phase space region with the color dipole approach, showing that the success of the CDM in this kinematic region is due to the all twist resummation embedded within it. Higher twist (HT) corrections in deeply inelastic scattering within the saturation model are defined in the literature [32, 33]. A twist analysis of the nucleon structure functions F_T and F_L at small values of the Bjorken variable x reveals that for F_L , the higher twist corrections are significant, while for $F_2 = F_T + F_L$ there is nearly complete cancellation of twist-4 corrections in F_T and F_L . A twist decomposition of the proton structure functions F_2 and F_L obtained from the Balitsky-Kovchegov (BK) equation using the Mellin representation of the scattering cross-sections at high energies based on the effects of non-linear small- x evolution of the gluon distribution within the collinear approximation framework is performed in Refs.[34, 35].

In Fig.3, we consider HT corrections as multiplicative shifts to the DIS structure function F_2 , represented by the ratio $\frac{\sigma_r(Q^2_s, Q^2)}{F_2(Q^2_s, Q^2)}$ in Eq. (16), which depends on $F_2(Q^2_s, Q^2)$. These HT corrections are parameterized as a phenomenological unknown function, and the values of the unknown parameters are determined through fits to experimental data [36–38]. It is common practice to adjust the leading-twist structure function by incorporating a term inversely proportional to Q^2 as a phenomenological power correction to account for HT effects in the structure function:

$$F_2(x, Q^2) = F_2^{LT}(x, Q^2) \left(1 + \frac{H_2(x)}{Q^2} \right). \quad (19)$$

Here, F_2^{LT} represents the leading twist contribution to F_2 , and the HT coefficient function $H_2(x)$ is parameterized as:

$$H_2(x) = \sum h_\alpha f_\alpha(x). \quad (20)$$

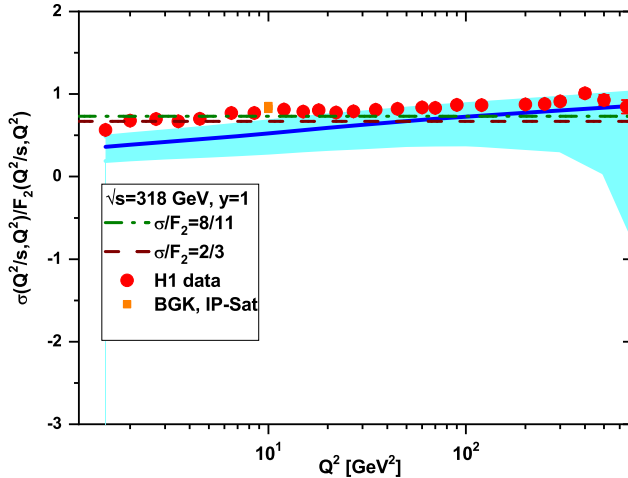


FIG. 2: We plot the ratio $\frac{\sigma_r}{F_2}(\frac{Q^2}{s}, Q^2)$ as a function of Q^2 at $y = 1$ for the HERA NC ep inclusive scattering data with $\sqrt{s} = 318$ GeV. The blue curves are extracted and compared with the results in Table VIII of Ref.[5] (red circles), as well as the BGK and IP-Sat models (yellow squares). The error bands correspond to the uncertainty in the parameterization of F_2 in [7]. The dipole upper bounds are represented by dashed and dashed-dot lines corresponding to $\rho = 1$ and $\frac{4}{3}$ in the CDM.

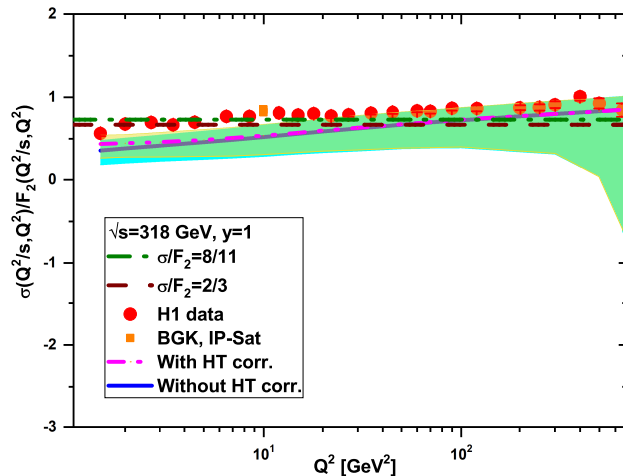


FIG. 3: We plot the ratio $\frac{\sigma_r}{F_2}(\frac{Q^2}{s}, Q^2)$ as a function of Q^2 at $y = 1$ for the HERA NC ep inclusive scattering data with $\sqrt{s} = 318$ GeV with (magenta-solid curve) and without (blue-solid curve) HT corrections. The results are compared with the data in Table VIII of Ref.[5] (red circles), as well as the BGK and IP-Sat models (yellow squares). The error bands correspond to the uncertainty in the parameterization of F_2 in [7] and the HT coefficient in [36–38]. The dipole upper bounds are represented by dashed and dashed-dot lines corresponding to $\rho = 1$ and $\frac{4}{3}$ in the CDM.

The parameters in this equation capture the HT effects in perturbative QCD, as discussed in Refs.[39, 40]. In the studies by authors in Refs.[36–38], the inclusion of an HT term in F_2 at low- x and low- Q^2 was investigated, revealing the necessity for $H_2 = 0.12 \pm 0.07$ GeV 2 for data with $y < 1$. In this figure (i.e., Fig.3), the ratio $\frac{\sigma_r}{F_2}(\frac{Q^2}{s}, Q^2)$ is plotted against Q^2 values at $x_{\min} = Q^2/s$ with and without HT corrections, compared with to results from Ref.[5] at $\sqrt{s} = 318$ GeV for $y = 1$, accompanied by data uncertainties, and CDM bounds. The impact of HT contribution on the ratio σ_r/F_2 is noticeable at low Q^2 values.

The HT coefficient of H_2 is determined through a fit to data over a wide range with $y < 1$. To demonstrate the HT effects in the ratio $\frac{\sigma_r}{F_2}(\frac{Q^2}{s}, Q^2)$ at $y = 1$, we calculated the ratio across a broad range of the HT coefficient. In Fig.4, we present the HT effects with $H_2 = 0.12, 0.5$, and 1 in comparison to the HERA data. We observe that the results

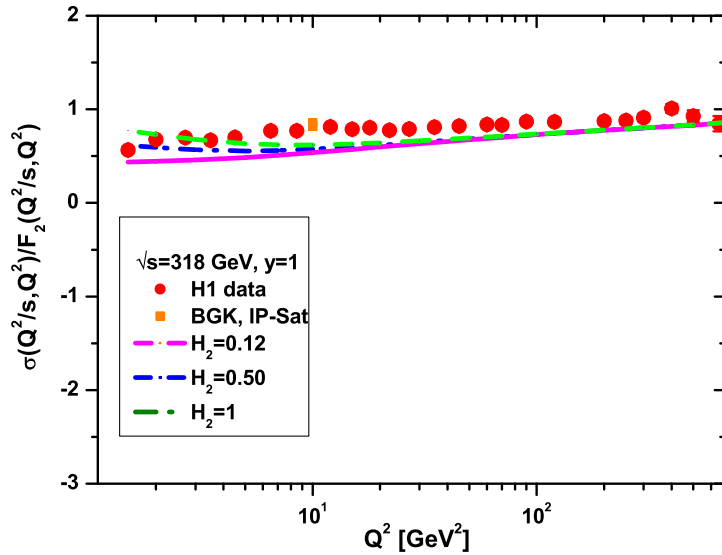


FIG. 4: We plot the ratio $\frac{\sigma_r}{F_2}(\frac{Q^2}{s}, Q^2)$ as a function of Q^2 at $y = 1$ for the HERA NC ep inclusive scattering data with $\sqrt{s} = 318$ GeV, incorporating HT corrections over a wide range of H_2 coefficients: $H_2 = 0.12$ (magenta-solid curve), 0.5 (blue-dashed-dot curve) and 1 (green-dashed curve). These results are compared to the data in Table VIII of Ref.[5] (red circles), as well as the BGK and IP-Sat models (yellow squares).

improve with increasing the HT coefficient due to high inelasticity, compared to the fit parameter $H_2 = 0.12$ at $y < 1$. The origin of this discrepancy is model-dependent, with all twist resummation improving the model as discussed in Refs.[34, 35].

Future measurements at the EIC and LHeC will be examined at upcoming colliders, serving as an interesting tool to investigate the longitudinal structure function at low x and moderate Q^2 . Our predictions for the ratio $\frac{\sigma_r}{F_2}(\frac{Q^2}{s}, Q^2)$ in the kinematic range of the EIC and LHeC colliders are shown in Fig.5. In this figure, the behavior of the ratio $\frac{\sigma_r}{F_2}(\frac{Q^2}{s}, Q^2)$ is considered with COM energies $\sqrt{s} = 89$ GeV and 1.3 TeV for the EIC and LHeC colliders respectively, and compared with the CDM bounds. The uncertainties in the ratio are due to the parametrization of the proton structure function and dependence on the model. For the EIC COM energy, results at $Q^2 > 100$ GeV² are out of reach due to large uncertainties in that domain. These results are independent of the mass number A and depend on the COM energies.

In conclusion, we studied the ratio $\frac{\sigma_r}{F_2}(x, Q^2)$ in momentum space using the Block-Durand-Ha parameterization of the proton structure function $F_2(x, Q^2)$. We developed a method to analyze high inelasticity, where $x_{Bj} = x_{min} = Q^2/s$. The extraction procedure was explained for analyzing the ratio of $\frac{\sigma_r}{F_2}(\frac{Q^2}{s}, Q^2)$ in the kinematical region of the H1 collaboration data and extended to high inelasticity data, which is determined by the effective parameters of the BDH parameterization and compared with the CDP bounds.

Our study further examines the ratio $\frac{\sigma_r}{F_2}(\frac{Q^2}{s}, Q^2)$, comparing it to H1 data and bounds from the color dipole model, showing strong agreement that supports the proposed methods. Additionally, we compared the results with the predictions of the BGK and IP-Sat models, finding good agreement with datasets across a wide range of Q^2 values. The HT corrections to the proton structure function by adding a simple form F_2*H_2/Q^2 to the ratio $\frac{\sigma_r}{F_2}(\frac{Q^2}{s}, Q^2)$ at low- x and low- Q^2 values are considered. These effects show that the ratio increases as the Q^2 value decreases at high inelasticity. The ratio $\frac{\sigma_r}{F_2}(\frac{Q^2}{s}, Q^2)$ at the EIC and the LHeC COM energies are considered in a wide range of Q^2 and compared with the CDM bounds.

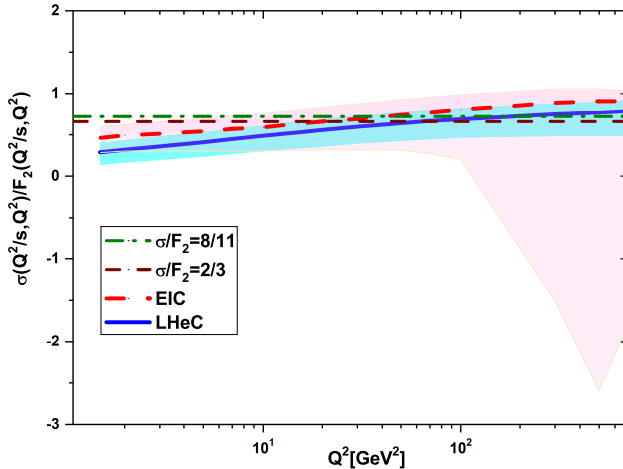


FIG. 5: We plot the ratio $\frac{\sigma_r}{F_2}(\frac{Q^2}{s}, Q^2)$ as a function of Q^2 at $y = 1$ for the EIC (red-dashed curve) and the LHeC (blue-solid curve) COM energies with $\sqrt{s} = 89$ GeV and 1.3 TeV respectively. The error bands correspond to the uncertainty in the parametrization of F_2 in [7]. The dipole upper bounds are represented by dashed and dashed-dot lines corresponding to $\rho = 1$ and $\frac{4}{3}$ in the CDM.

ACKNOWLEDGMENTS

The author is thankful to Razi University for the financial support provided by this project.

TABLE I: The effective parameters in the BDH expression for $F_2(x, Q^2)$ at small x for $0.15 \text{ GeV}^2 < Q^2 < 3000 \text{ GeV}^2$ provided by the following values. The fixed parameters are defined by the Block-Halzen fit to the real photon-proton cross section as $M^2 = 0.753 \pm 0.068 \text{ GeV}^2$, $\mu^2 = 2.82 \pm 0.290 \text{ GeV}^2$, and $a_{00} = 0.2550 \pm 0.016$ [7].

parameters	value
n	$n = 11.49 \pm 0.99$
λ	2.430 ± 0.153
a_{01}	$1.475 \times 10^{-1} \pm 3.025 \times 10^{-2}$
a_{10}	$8.205 \times 10^{-4} \pm 4.62 \times 10^{-4}$
a_{11}	$-5.148 \times 10^{-2} \pm 8.19 \times 10^{-3}$
a_{12}	$-4.725 \times 10^{-3} \pm 1.01 \times 10^{-3}$
a_{20}	$2.217 \times 10^{-3} \pm 1.42 \times 10^{-4}$
a_{21}	$1.244 \times 10^{-2} \pm 8.56 \times 10^{-4}$
a_{22}	$5.958 \times 10^{-4} \pm 2.32 \times 10^{-4}$

[1] C. Adloff et al. [H1 collaboration], Eur.Phys.J.C **21**, 33 (2001).
[2] F. D. Aaron et al. [H1 and ZEUS collaboration], JHEP **01**, 109 (2010).

- [3] H. Abramowicz et al. [H1 and ZEUS collaboration], *Eur. Phys. J. C* **75**, 580 (2015).
- [4] P. Agostini et al. [LHeC Collaboration and FCC-he Study Group], *J. Phys. G: Nucl. Part. Phys.* **48**, 110501 (2021).
- [5] F.E.Taylor, *Phys. Rev.D* **111**, 052001 (2025).
- [6] T. Lappi, H. Mantysaari, H. Paukkunen, and M. Tevio, *Eur. Phys. J. C* **84**, 84 (2024).
- [7] M. M. Block, L. Durand and P. Ha, *Phys.Rev.D* **89**, 094027 (2014).
- [8] Martin M. Block, Loyal Durand and Douglas W. McKay, *Phys.Rev.D* **79**, 014031 (2009) .
- [9] Martin M. Block, Loyal Durand, Phuoc Ha and Douglas W. McKay, *Phys.Rev.D* **83**, 054009 (2011).
- [10] Martin M. Block, Loyal Durand, Phuoc Ha and Douglas W. McKay, *Phys.Rev.D* **84**, 094010 (2011).
- [11] Martin M. Block, Loyal Durand, Phuoc Ha and Douglas W. McKay, *Phys.Rev.D* **88**, 014006 (2013).
- [12] G. R. Boroun and P. Ha, *Phys. Rev. D* **109**, 094037 (2024).
- [13] G. R. Boroun and P. Ha, *Phys. Rev. D* **111**, 034012 (2025).
- [14] C. Ewerz et al., *Phys.lett.B* **720**, 181 (2013).
- [15] C. Ewerz and O. Nachtmann, *Phys. Lett. B* **648**, 279 (2007).
- [16] M. Niedziela and M. Praszalowicz, *Acta Physica Polonica B* **46**, 2018 (2015).
- [17] M. Kuroda and D. Schildknecht, *Phys. Lett. B* **618**, 84 (2005).
- [18] M. Kuroda and D. Schildknecht, *Phys. Lett. B* **670**, 129 (2008).
- [19] M. Kuroda and D. Schildknecht, *Phys. Rev. D* **85**, 094001 (2012).
- [20] M. Kuroda and D. Schildknecht, *J. Mod. Phys. A* **31**, 1650157 (2016).
- [21] N. N. Nikolaev and B. G. Zakharov, *Phys. Lett. B* **332**, 184 (1994).
- [22] N. N. Nikolaev and B. G. Zakharov, *Z. Phys. C* **49**, 607 (1991).
- [23] N. N. Nikolaev and B. G. Zakharov, *Z. Phys. C* **53**, 331 (1992).
- [24] G.R.Boroun and B.Rezaei, *Phys. Lett. B* **816**, 136274 (2021).
- [25] G.R.Boroun, M. Kuroda and D. Schildknecht, *Eur. Phys. J. Plus* **140**, 1149 (2025).
- [26] G.R.Boroun and B.Rezaei, *Phys.Rev.C* **103**, 065202 (2021).
- [27] G.R.Boroun and B.Rezaei, *Nucl.Phys.A* **990**, 244 (2019).
- [28] G.R.Boroun, *Eur.Phys.J.A* **57**, 219 (2021).
- [29] G.R.Boroun, *Phys.Rev.D* **109**, 054012 (2024).
- [30] A. Accardi et al., *Eur. Phys. J. A* **52**, 268 (2016).
- [31] R. Abdul Khalek et al., *Nucl. Phys. A* **1026**, 122447 (2022).
- [32] J.Bartels, K. Golec-Biernat, and L.Motyka, *Phys.Rev.D* **81**, 054017 (2010).
- [33] J.Bartels, K. Golec-Biernat, and K.Peters, *Eur.Phys.J.C* **17**, 121 (2000).
- [34] L.Motyka and M.Sadzikowski, *Eur. Phys. J. C* **83**, 1062 (2023).
- [35] L.Motyka and M.Sadzikowski, *Acta Physica Polonica B* **45**, 2079 (2014).
- [36] A.M. Cooper-Sarkar, *PoS DIS2016* (2016) 013.
- [37] I. Abt, et al., *Phys.Rev.D* **94**, 034032 (2016) .
- [38] F.D. Aaron, et al., H1 Collaboration, *Eur. Phys. J. C* **63**, 625 (2009).
- [39] H. Khanpour, A. Mirjalili, S. Atashbar Tehrani, *Phys. Rev. C* **95**, 035201 (2017).
- [40] Richard D. Ball, A. Chiefa, and R. Stegeman, *arXiv[hep-ph]:2511.14387*.
- [41] L.P. Kaptari, et al., *Phys.Rev.D* **99** (2019) 096019.
- [42] H1 Collab. (V. Andreev et al.), *Eur.Phys.J.C* **74** (2014) 2814.
- [43] M.A.G.Aivazis et al., *Phys.Rev.D* **50**, 3102 (1994).
- [44] D.A.Fagundes and M.V.T.Machado, *Phys.Rev. D* **107**, 014004 (2023).
- [45] H. Kowalski and D. Teaney, *Phys. Rev. D* **68**, 114005 (2003).
- [46] J. Bartels, K. J. Golec-Biernat, and H. Kowalski, *Phys. Rev. D* **66**, 014001 (2002).